Role of the recoil ion in single-electron capture and single-ionization processes for collisions of protons with He and Ar atoms

P. Focke,[1] R. E. Olson,[2] N. D. Cariatore,[1,3] M. Alessi,[4] and S. Otranto[3]

[1]*Centro Atómico Bariloche, Av. Bustillo 9500, 8400 S. C. de Bariloche, Argentina*

[2]*Physics Department, Missouri University of Science and Technology, Rolla Missouri 65409, USA*

[3]*Instituto de Física del Sur (IFISUR), Departamento de Física, Universidad Nacional del Sur (UNS), CONICET, Av. Alem 1253 B8000CP Bahía Blanca, Argentina*

[4]*INVAP SE, Av. L. Piedrabuena 4950, 8400CPV, S. C. de Bariloche, Argentina*

(Received 14 March 2017; published 23 May 2017)

In this work the single-electron capture and single-ionization processes are studied for proton collisions with He and Ar atoms at impact energies in the range 25–100 keV. Classical trajectory Monte Carlo simulations are benchmarked against experimental data obtained at the reaction microscope in Bariloche, Argentina, which employs the cold target recoil-ion momentum spectroscopy technique. Special emphasis is placed on describing the momentum transfer to the recoil ion for these collision systems.

DOI: 10.1103/PhysRevA.95.052707

I. INTRODUCTION

During the past two decades, the study of collision processes involving charged particles or photons with atoms and molecules has been revitalized through the implementation of reaction microscopes at different laboratories worldwide. These are based on the cold target recoil-ion momentum spectroscopy (COLTRIMS) technique which allows a kinematically complete description of the collision process [1–3]. This technique is also the basis for subsequent developments like the magneto-optical target recoil-ion momentum spectroscopy (MOTRIMS) technique [4–6]. In the latter, the RIMS technique is combined with a target that is laser cooled and trapped in a magneto-optical trap. Together, the techniques have allowed the exploration of the various physical mechanisms that mediate collision processes with an unprecedented level of detail.

In this context, differential cross-sections in the projectile scattering angle and/or the transverse recoil-ion momentum provide a unique insight into the collision process and can reveal footprints of the many physical mechanisms. As an example, for charge exchange we can cite the atomic-size Fraunhofer-type diffraction patterns observed in 0.45–1 keV/amu $Li^+ + Na$ collisions [4] and the recent identification of electron saddle swaps oscillations in angular-differential charge exchange cross sections in 1–10 keV/amu $Ne^{8+} + Na(3s)$ collisions [7]. These oscillations, which on a quantal description originate from phase interference of two paths leading to a common final state, on a classical basis relate to the electron swapping centers during the collision. These angular-differential analyses become more complex for the single-ionization process, provided that the angular scattering of the projectile cannot be directly determined from the recoil-ion momentum and the emitted electron momentum must also be considered.

In this work, we present single-electron capture COLTRIMS data measured at the Centro Atómico Bariloche, Argentina, for collisions of protons with He and Ar targets. Present data are contrasted to classical trajectory Monte Carlo (CTMC) simulations [8]. Theoretical studies for the ionization process, which cannot be addressed with the present experimental setup, are also included. The proton-He system has been studied in detail for many years and is used to benchmark the experimental techniques that were developed for the proton-Ar system.

Motivation for studying collisions involving Ar targets arises from the need to understand collisions involving Ar for efficient heat transfer in the divertor region of next-generation nuclear fusion reactors such as the ITER reactor being constructed in France [9]. In order to uniformly illuminate and heat the divertor where heat is transferred for electrical power generation, heavy rare gases such as Ar are injected to provide ions and atoms that will undergo charge transfer and relax via photon emission, thus reducing the possibility of having burnthrough by the plasma of the container wall. To lowest order, proton (or deuteron) collisions with Ar need to be studied in detail.

The organization of this paper proceeds with Sec. II where the experimental procedure is described. In Sec. III, we present the main features of our CTMC simulations. Results are discussed in Sec. IV. Finally, conclusions and outlook are given in Sec. V.

II. EXPERIMENT

The measurements have been performed with the COLTRIMS experiment installed at the 20-300 kV Cockroft-Walton accelerator in Bariloche, Argentina. A detailed account of the apparatus and procedures used to process the measured data has been described in detail elsewhere [10]. A brief description will be given now taking into account changes done for the present measurements. A proton beam of 25, 50, and 80 keV energy collided with an atomic beam of either He or Ar.

The recoil-ion momentum of the ionic target atoms was measured in coincidence with emerging neutral projectiles selecting by this way the single-capture process. The proton beam delivered from the accelerator, magnetically selected and collimated, is guided to the collision chamber where it crosses perpendicularly the atomic target gas jet. The emergent projectiles are charge-state analyzed and recorded by a channeltron detector. The collision region is located

inside the spectrometer where a homogeneous electric field, perpendicular to the projectile beam and the gas jet, extracts the recoil ions and projects them onto a two-dimensional position- and time-sensitive detector with a delay-line anode [microchannel plates (MCPs)]. The acceleration section in the spectrometer is followed by a field-free drift region that provides time-focusing operation.

The recoil ions are detected in coincidence with a selected charge state from the projectile detector. The gas jet is supplied by adiabatic expansion through a single-stage supersonic nozzle followed by a skimmer. The target system is differentially pumped in order to maintain a good vacuum in the collision chamber. There is the possibility to use a gas reservoir provided with a Cu cold finger mounted on a cell that can be filled with liquid N_2 in order to precool the target gas before expansion. Measuring the recoil-ion hit position and the time of flight, the three components of the recoil-ion momentum after the collision can be determined [10]. The coordinate system used for the present measurements has its origin placed at the collision region, with the z axis along the incident projectile beam, the y axis along the gas jet, and the x axis along the spectrometer axis in the direction of the electric extraction field. The low electric fields used were typically 2 V/cm along a 4-cm extraction region.

An issue to take into account is an estimate of the initial random momentum of the target atoms. For an Ar gas target with a driving pressure at the reservoir of 1270 Torr and at room temperature, after adiabatic expansion through the supersonic nozzle, we estimate, using expressions from Ref. [11], a random momentum spread $\Delta p_y = 0.9$ a.u. at a terminal momentum of $p_{\text{term}} = 18.4$ a.u. After expansion the Ar target is at nearly 1.7 K. On the other hand, due to collimation of the target gas jet by the skimmer we estimate a residual momentum spread along the z of $\Delta p_z = 0.46$ a.u. Due to additional collimation of the projectile beam, we get along x a $\Delta p_x = 0.21$ a.u. These figures result from collimation effects on a molecular beam (geometrical cooling) assuming a point gas source located close to the nozzle exit [1].

An important difference between the two targets under consideration is their behavior with respect to the precooling stage. In contrast to He, the precooling stage cannot be implemented for Ar since it liquefies at the reservoir. The avoidance of the precooling stage drastically affects the cylindrical symmetry expected for the transverse component of the recoil momentum ($p^2_{\text{rec-}t} = p^2_{\text{rec-}x} + p^2_{\text{rec-}y}$). To circumvent this issue, and provided that the transverse component that is expected to be thermally affected is that corresponding to the jet direction (y coordinate), a back-projection procedure of the $p_{\text{rec-}x}$ component based on the inverse Abel transform is performed to recover the cylindrical symmetry [12–14]. This procedure has also been implemented in MOTRIMS studies which are based in the detection of one of the transverse recoil-ion momentum components [15].

In Fig. 1 we test the back-projection procedure on our single-electron capture results for 80 keV proton collisions on He by showing the two-dimensional distribution of recoil-ion momenta in the transverse plane. The resulting data are contrasted to those obtained with the precooling stage. When the precooling stage is not implemented [Fig. 1(a)], there is a clear distortion with respect to the cylindrical symmetry obtained once the precooling stage is incorporated [Fig. 1(b)]. This asymmetry effect stems from the initially random momentum present in the target which cannot be canceled by solely relying on the adiabatic expansion of the target jet. In this sense, it can be seen that the $p_{\text{rec-}x}$ distributions with and without precooling stage are in very good agreement, while the $p_{\text{rec-}y}$ distribution displays a much wider profile when the precooling stage is not implemented [Fig. 1(c)]. The implementation of the back-projection procedure [Fig. 1(d)] leads to very good agreement at the $p_{\text{rec-}t}$ distribution level, and provides confidence on its use to explore collision processes on a target such as argon, for which the precooling stage is not an option.

III. THEORY

In this work the three-body CTMC model in its microcanonical formulation is employed [8]. Hamilton's equations are numerically solved for the mutually interacting three-body system in which the active electron is assumed to interact with the He and Ar cores under the potential model developed by Green *et al.* from Hartree-Fock calculations [16] and later on generalized by Garvey *et al.* [17]:

$$V(r) = \frac{(N-1)[1-\Omega(r)] - Z}{r}, \tag{1}$$

$$\Omega(r) = \left[\left(\frac{\eta}{\xi}\right)(e^{\xi r} - 1) + 1\right]^{-1}. \tag{2}$$

The corresponding parameters are $Z = 2, N = 2, \xi = 2.625, \eta = 1.77$ and $Z = 18, N = 18, \xi = 0.957, \eta = 3.5$ for He and Ar, respectively. The electron evolving in these model potentials sees an asymptotic core charge of $+1$ which gradually increases towards the respective nuclear charges $+2$ and $+18$ as the electron-core distance tends to zero.

To deal with the multielectronic character of the target, we present theoretical results within the independent event (IEV) and independent electron (IEL) models. In these models the explicit reaction probabilities for He and Ar targets are given by

$$P_j^{\text{Ar}}(b) = P_j^{3p}(b)\left[1 - P_{\text{SC}}^{3p,i}(b) - P_{\text{SI}}^{3p,i}(b)\right]^5 \times \left[1 - P_{\text{SC}}^{3s,i}(b) - P_{\text{SI}}^{3s,i}(b)\right]^2, \tag{3}$$

$$P_j^{\text{He}}(b) = P_j^{1s}(b)\left[1 - P_{\text{SC}}^{1s,i}(b) - P_{\text{SI}}^{1s,i}(b)\right]. \tag{4}$$

In these expressions j represents electron capture (SC) or ionization (SI) depending on the case and i refers to the reaction probabilities corresponding to the original target atom (IEL) or the $+1$ ion (IEV). Since we are interested in the analysis of differential cross sections within the IEV and IEL models, we have filtered our event files by means of a Monte Carlo procedure. First, the reaction probabilities shown in Eqs. (3) and (4) have been determined as a function of the impact parameter b. Next, for each electron capture or ionization event recorded from our CTMC simulation we check its corresponding impact parameter b and sort a random number ξ in the (0,1) interval. If ξ is lower than $[1 - P_{\text{SC}}^{3p,i}(b) - P_{\text{SI}}^{3p,i}(b)]^5 [1 - P_{\text{SC}}^{3s,i}(b) - P_{\text{SI}}^{3s,i}(b)]^2$ for

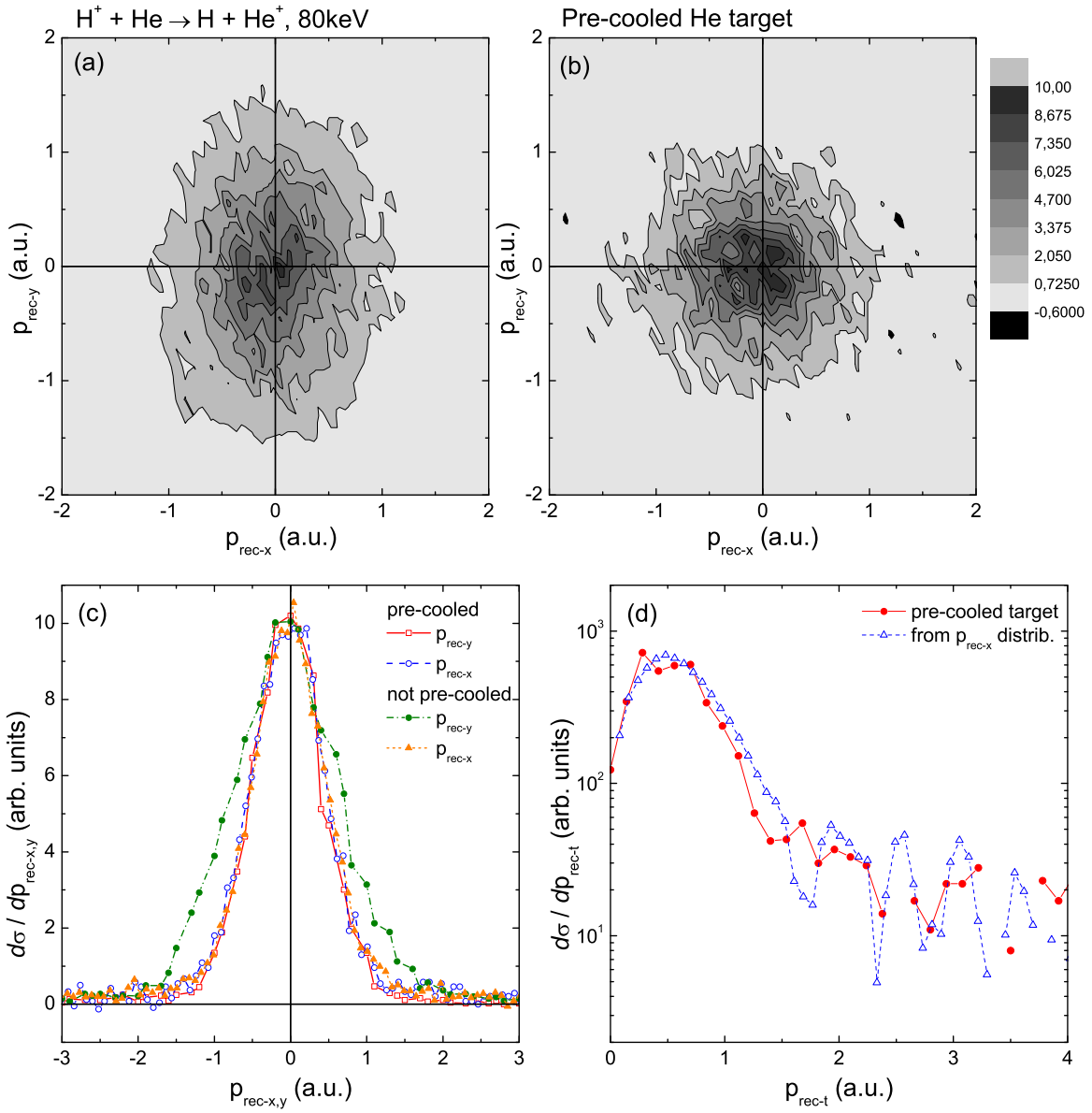

FIG. 1. Transverse momentum distributions for $H^+ + He$ collisions at 80 keV: (a) adiabatic expansion cooling only, (b) with additional precooling stage, (c) projected distributions along the transverse directions (x and y axes), (d) transverse momentum distribution.

Ar or $[1 - P_{SC}^{1s,i}(b) - P_{SI}^{1s,i}(b)]$ for He, then the event is kept. Otherwise it is rejected in order to preserve unitarity of the transition probabilities.

Since the present work is focused on the single-electron capture and single-ionization channels, electron loss from Ar($3s$) has not been considered since it is expected to lead to double electron removal, mainly transfer ionization, after stabilization.

IV. RESULTS

A. He target

First we will consider the He target for which differential cross sections for electron capture as a function of the projectile scattering angle have been available from the pioneering work of Martin *et al.* [18] which, throughout the past three decades, has been used to benchmark the experimental data from several laboratories [19,20]. In Fig. 2 we show the target recoil-ion transverse momentum distribution for the single-electron capture channel in 50, 80, and 100 keV H^+ collisions on He. At 50 keV, the present data are found in very good agreement with the absolute cross sections of Martin *et al.*, which have been converted from differential in terms of the scattering angle of the projectile to differential in the recoil ion $p_{\text{rec-}t}$. The present relative experimental data have been normalized to the absolute data of Martin *et al.* at their peak value. Likewise, the CTMC-IEV and CTMC-IEL results have been normalized to the peak value by multiplying factors (stated in the caption) to help identify major differences in shape. The Hartree-Fock Compton profile for He($1s$) given by Biggs *et al.* [21] is also included and shows a wider structure than that evidenced by the experimental and theoretical data. While it should be stated that the present CTMC model is expected to underestimate to some extent the low-$p_{\text{rec-}t}$

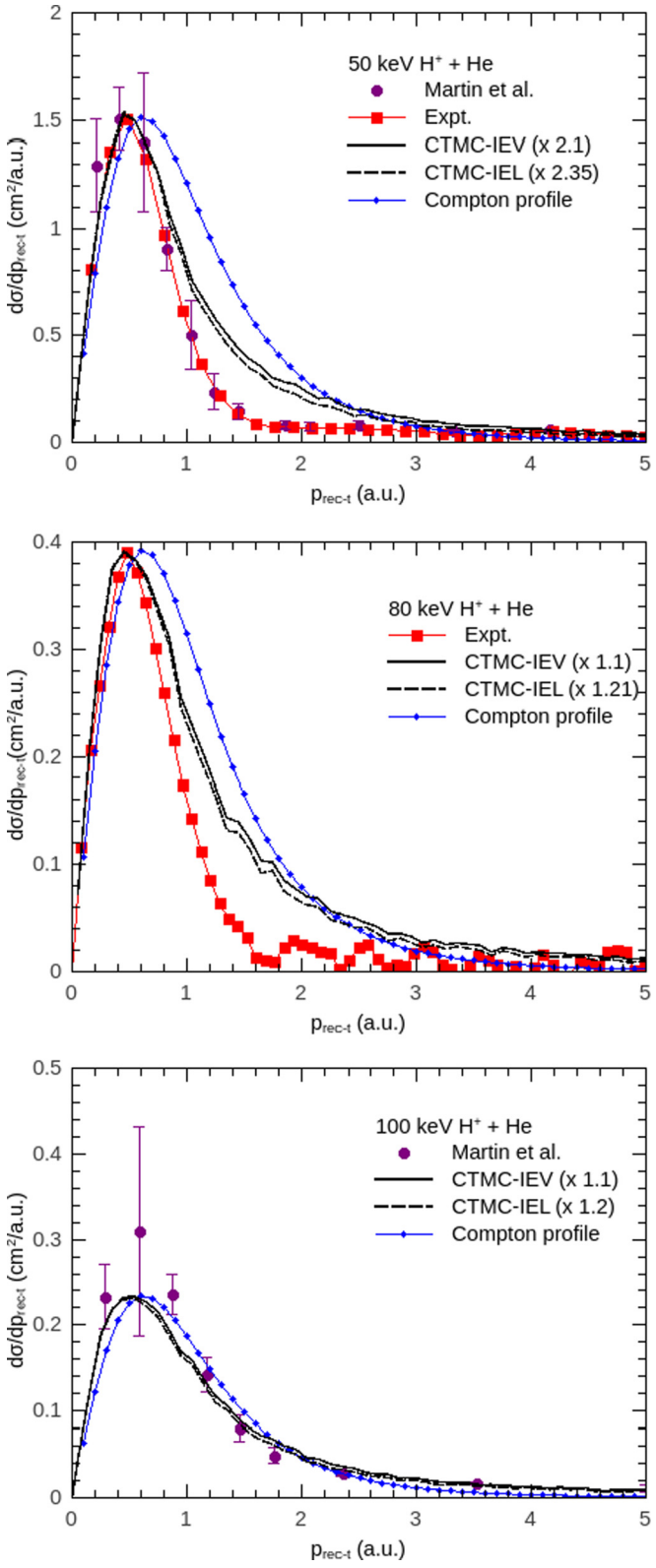

FIG. 2. Recoil-ion transverse momentum distributions of the single-electron capture process for $H^+ + He$ collisions at 50, 80, and 100 keV.

region due to the sharp cutoff in the microcanonical radial distribution, it seems clear from the experimental data that the capture process is fed mainly with those target electrons which have small transverse momentum when the removal takes place.

At 80 keV, we find a similar situation. Experiment and theory predict distributions that are both narrower than the Compton profile. At 100 keV the present CTMC models are in agreement with the data of Martin *et al.* [18] and smaller scaling factors are needed compared to the 50 and 80 keV cases. Compared to the 80 keV case the experimental $p_{\text{rec-}t}$ distribution widens, a fact that can be attributed to the increasing role of the ionization channel. At this impact energy, the single-electron capture is fed from collisions involving low impact parameters, a range over which the target electrons cover their whole accessible $p_{\text{elec-}t}$ range. As a result, the recoil-ion transverse momentum is reflecting the initial target Compton profile in the transverse direction. In fact, an Abel transform over the theoretical data shown predicts a Compton profile with a full width at half maximum (FWHM) of 1.452 a.u. which compares well to the 1.58 a.u. obtained from Hartree-Fock calculations [21], the 1.5 a.u. value from Hicks which explicitly includes the electron-electron interaction in the target [22], and the experimental value of 1.5 a.u. from DuMond and Kirkpatrick [23] in their study of the structure and shift of the Compton line of He.

Now turning to the single-ionization process, COLTRIMS data from Weber *et al.* [24] explicitly display an abrupt rise in the recoil-ion longitudinal momentum distribution which had been theoretically predicted by Rodríguez *et al.* [25] in 1995. This abrupt rise occurs at $p_{\text{rec-min}} = -v_p/2 - E_{\text{bind}}/v_p$ and can be associated to the electron capture to the continuum (ECC) process where the captured electron matches the velocity of the projectile. The structure went unnoticed during the initial experiments measured by the mid-1990s for the present collision system [26]. Impact energies had to be lowered below 200 keV/amu before it could be experimentally found in 100–250 keV/amu D^+ collisions on He [24]. In Fig. 3 we show the theoretical double differential cross sections (DDCSs) $d^2\sigma/(d\,p_{\text{rec-}z}\,d\,p_{\text{rec-}t})$ for 50, 80, and 100 keV H^+ collisions on He. Differences arising from the IEV and IEL formulations are indistinguishable in this representation.

As the impact energy increases, so does the range of $p_{\text{rec-}z}$ comprised between the ECC and the electron capture to the target (ECT) (soft collision electron emission) mechanisms. Weber *et al.* relate the fact that their DDCS peak at small values for the recoil-ion momentum with the emission of low-energy electrons. Since in principle the projectile can also play a role in terms of the momentum exchange that takes place during the collision, we also plot $d^2\sigma/(d\,p_{\text{elec}}\,d\,p_{\text{rec}})$ to check whether their conclusion is consistent with our theoretical results. At the impact energies explored, the doubly differential cross section is dominated by ionization events corresponding to small recoil momenta and electron energies lower than about 30, 42, and 55 eV, respectively. From our results we infer that the recoil ion plays an active role in the emission of energetic electrons. This is expected since those events are associated with small impact parameters in which the internuclear interaction cannot be neglected.

In Fig. 4 we show the CTMC-IEV longitudinal and transverse momentum distributions and compare them to the Compton profile. Distributions within the CTMC-IEL model mainly differ from those shown in an overall

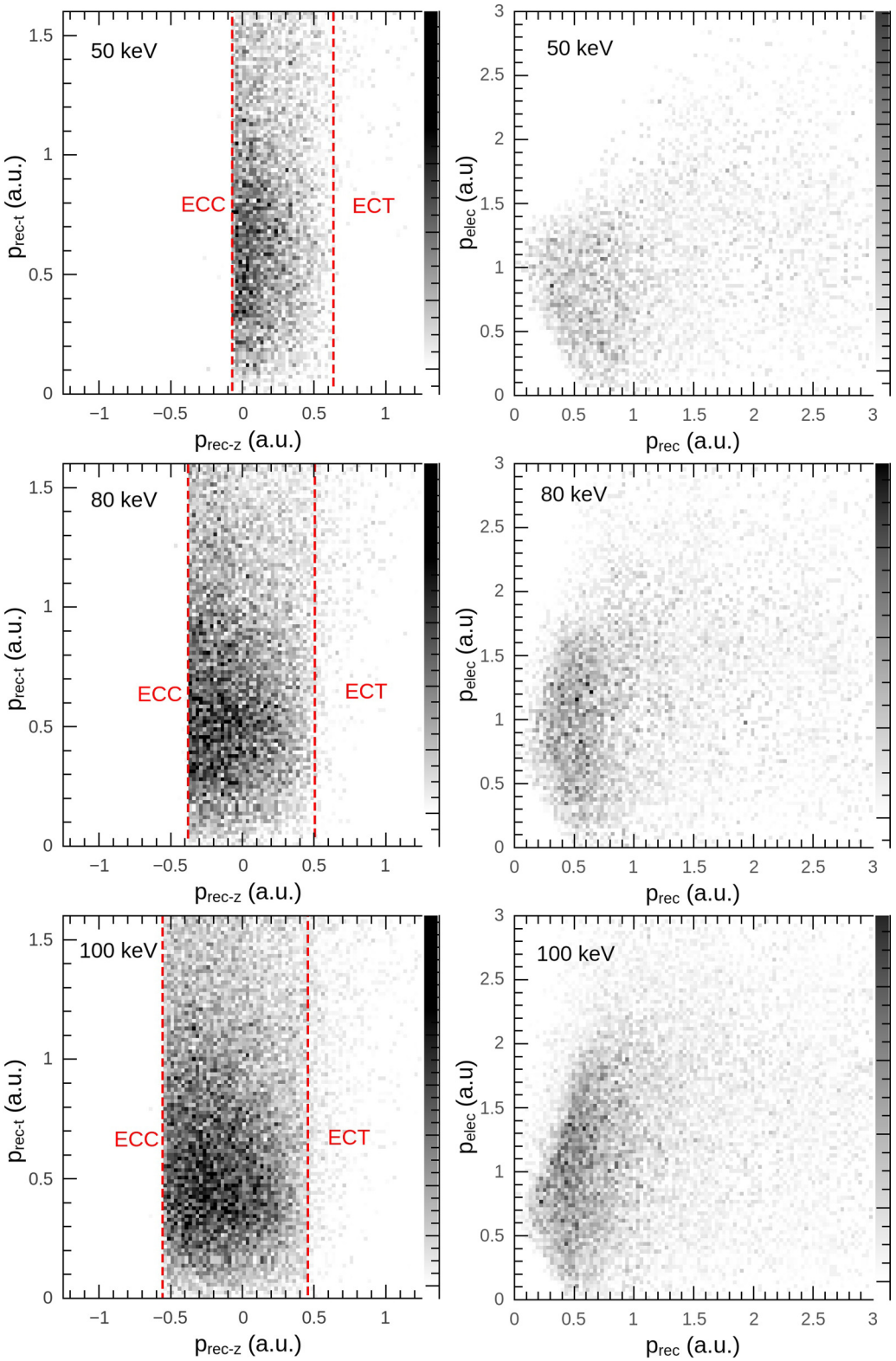

FIG. 3. Theoretical $d^2\sigma/(d\,p_{\rm elec}d\,p_{\rm rec})$ and $d^2\sigma/(d\,p_{\rm rec\text{-}z}d\,p_{\rm rec\text{-}t})$ of the single-ionization process for 50, 80, and 100 keV H^+ collisions on He. The dashed lines indicate the recoil-ion longitudinal momentum values associated to the electron capture to the continuum (ECC) and electron capture to the target (ECT) mechanisms. Predictions within the IEV and IEL models are indistinguishable in this plot.

scaling factor and for clarity purposes are not included. The recoil-ion longitudinal distributions exhibit the sharp rise at $p_{\rm rec\text{-}min} = -v_p/2 - E_{\rm bind}/v_p$ which is associated with the ECC process [24]. This structure moves towards the negative $p_{\rm rec\text{-}z}$ direction for increasing impact energies, leading to an overall widening of the distribution. Cases explored show that this distribution is narrower than the Compton profile, indicating that the electron emission is mediated by the

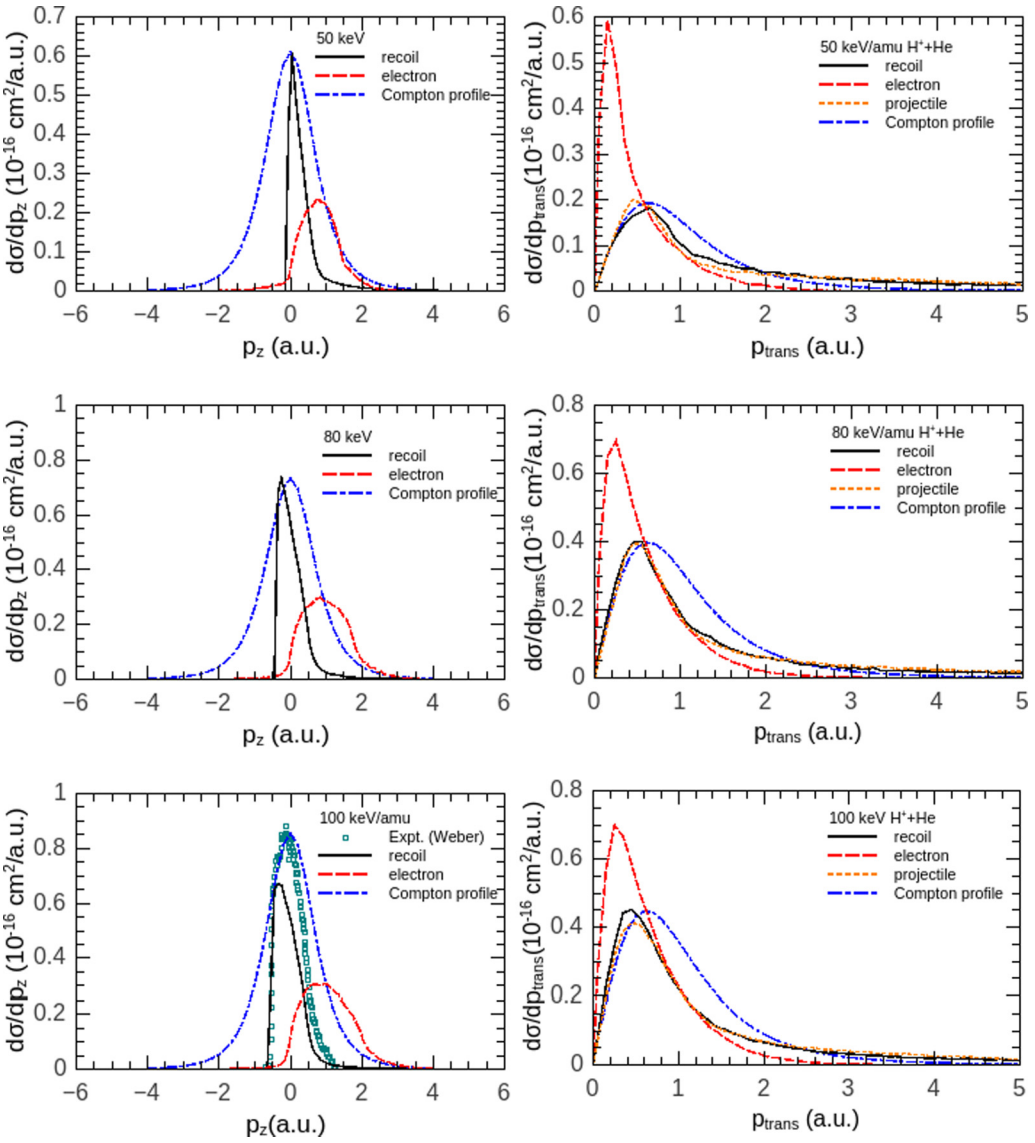

FIG. 4. CTMC-IEV longitudinal and transverse momentum distributions of the single-ionization process for 50, 80, and 100 keV H^+ collisions on He. The experimental longitudinal recoil-ion momentum distribution of Weber *et al.* [24] for 100 keV/amu d^+ collisions on He is included for comparison.

smaller recoil-ion longitudinal momentum components. At 100 keV, our theoretical data are benchmarked against the experimental data from Weber *et al.* [24] for 100 keV/amu d^+ collisions on He. Good agreement is obtained even though the theoretical results underestimate the ECT region. This is probably related to limitations detected in the classical model to fully reproduce the width of the recoil-peak structure in fully differential studies [27]. Concerning the longitudinal momentum distribution for the emitted electron, it can be seen in all cases that most of the events are comprised of velocities lower than that corresponding to the projectile and structures peak at longitudinal momentum values close to $v_p/2$. In the transverse momentum distributions, electrons tend to be emitted with small momentum transfers. Hence, the recoil-ion momentum in this direction is nearly identical to that obtained for the projectile indicating that the projectile angular dispersion is mainly a consequence of the internuclear interaction. Moreover, these distributions are in fair agreement with the Compton profile clearly indicating that the angular scattering of the projectile is to a great extent determined by the momentum distribution of the electron in its initial bound state.

B. Ar target

We now consider the single-electron capture process for the Ar target. Measurements were carried out at proton impact energies of 25, 50, and 80 keV. The experimental data were normalized to the single-capture data from Ref. [28] which include the contributions from the transfer ionization channel and report an overall uncertainty of ±25%. An additional weighting factor is given by the fraction of events leading to Ar^+ ions in our coincidences with H^0. The Ar recoil-ion charge-state spectrum is shown in Fig. 5 at an impact energy of 25 keV. These factors are given by 0.848, 0.792, and 0.7633 at 25, 50, and 80 keV respectively. Finally, the upper limit

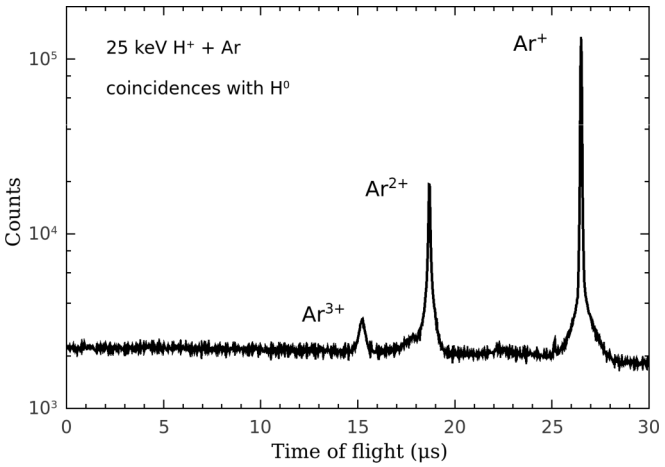

FIG. 5. Ar^{q+} ion spectra obtained in coincidence with H^0 at a proton impact energy of 25 keV.

of detection of the p_t value of our recoil ions is 10.77 a.u. at 25 and 50 keV and 8 a.u. at 80 keV. From our CTMC simulations we find that about 5% of the collected events at 25 and 50 keV escape the experimentally accessible p_t region, a fraction that increases to about 9% at 80 keV. The above information was then used to obtain the absolute cross sections for the experimental data.

In Fig. 6 we show the target recoil-ion transverse momentum distribution for the single-electron capture channel in 25, 50, and 80 keV H^+ collisions on Ar. The error bar associated with the peak value is incorporated to reflect the ±25% uncertainty of the total cross sections from Ref. [28] used to normalize our data. While at 25 keV we observe that the theoretical distribution peaks at a smaller $p_{\text{rec-}t}$ value than the experimental data, at 50 and 80 keV good agreement between theory and experiment is obtained at the peak position. In all cases, our theoretical results lead to a wider structure compared to the experimental data. This behavior reflects to some extent the underestimation in our microcanonical ensemble of low-$p_{\text{rec-}t}$ events arising from large impact parameters and from the fact that we do not explicitly account for the transfer ionization process which removes flux from single capture and dominates at the small impact parameters that correspond to large momentum transfer.

In contrast to our findings for the He target, as the impact energy increases the scaling factors needed to normalize our theoretical results to the data peak values increase with increasing impact energies. Moreover, our theoretical and experimental results do not converge to the Hartree-Fock Compton profile for Ar($3p$) from Ref. [21]. Preliminary experimental tests for proton impact energies up to 200 keV confirm this trend. To investigate this point, in Fig. 7 we show the impact parameter distributions within the CTMC-IEV and CTMC-IEL models for single capture in 80 keV H^+ collisions on He and Ar. It can be seen that the maximum contribution to charge exchange in Ar arises from larger impact parameters compared to He. This shift forward can be associated with the large asymmetry between the target charge seen by the electron at low impact parameters and the impinging projectile charge. In other words, at low impact parameters the electron-target

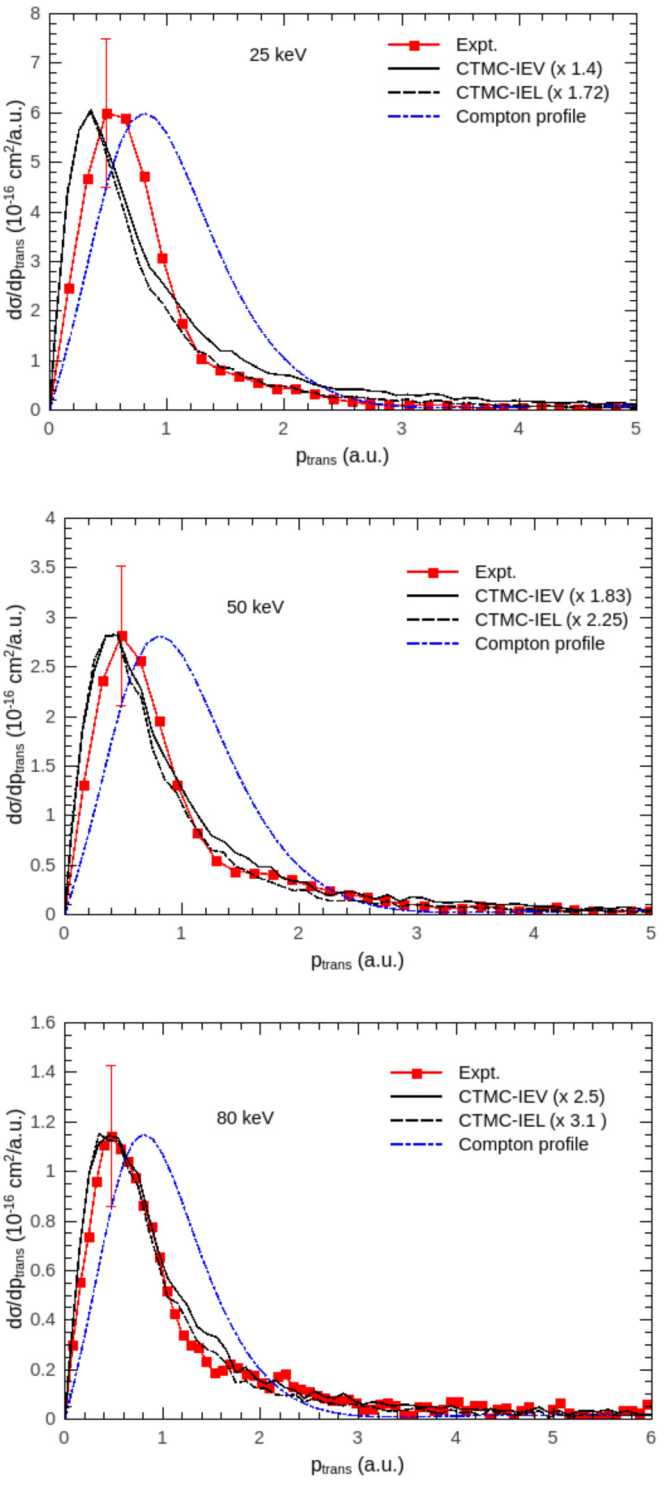

FIG. 6. Recoil-ion transverse momentum distributions of the single-electron capture process for $H^+ + Ar$ collisions at 25, 50, and 80 keV.

ion interaction is much stronger than the electron-projectile interaction, diminishing the probability of having electron capture.

Since capture at large impact parameters is associated with low transverse momentum values for the target electron, we infer that only a fraction of the Compton profile of the target

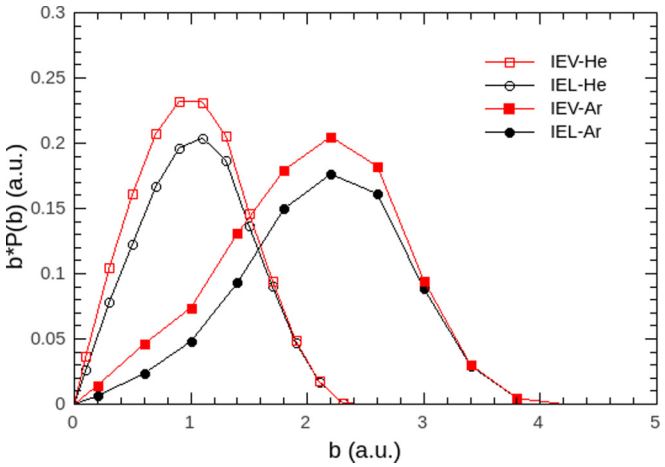

FIG. 7. Theoretical impact parameter distributions for single-electron capture at 80 keV H^+ impact collisions on He and Ar.

electron actually contributes to electron capture, a situation that is not expected to change drastically at larger impact energies. This situation is more clearly illustrated in Fig. 8, in which we show the CTMC events plot for $p_{\text{rec-}t}$ as a function of b at the same impact energy of 80 keV. It can be seen that the peak of the $p_{\text{rec-}t}$ distribution is mainly constructed from contributions over a broad range of impact parameters from 1.75 to 3.5 a.u. The fact that scaling factors had to be used for He and Ar targets in our IEV and IEL models indicates for proton impact a systematic underestimation of one-electron processes at the expense of overestimating multiple-electron processes.

Turning to the single-ionization process, in the first column of Fig. 9 we show the theoretical double differential cross sections (DDCSs) $d^2\sigma/(d\,p_{\text{rec-}z}d\,p_{\text{rec-}t})$ and $d^2\sigma/(d\,p_{\text{elec}}d\,p_{\text{rec}})$ for 50, 80, and 100 keV H^+ collisions on Ar. At first sight, our theoretical results display trends which are similar to those presented and discussed for the He target in Fig. 3. However,

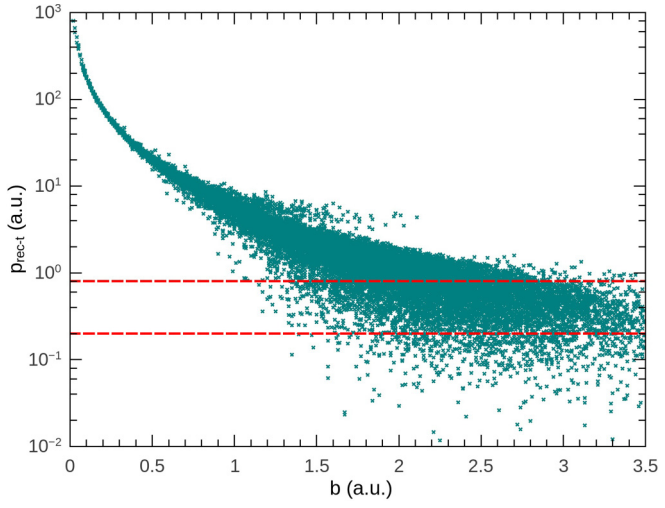

FIG. 8. CTMC events plot of $p_{\text{rec-}t}$ as a function of b for 80 keV H^+ + Ar collisions leading to electron capture. The dashed lines indicates the region 0.2–0.8 a.u. at which the maximum of the $p_{\text{rec-}t}$ distribution shown in Fig. 6 is predicted. Predictions within the IEV and IEL models are indistinguishable in this plot.

we now focus on the information shown by $d^2\sigma/(d\,p_{\text{elec}}d\,p_{\text{rec}})$, a representation to which not much attention has been paid so far. Two zones are distinguished which we have denoted as A and B and that we analyze in what follows.

The complete absence of ionization events in region A of the p_{elec}-p_{rec} space can be understood in terms of the minimum amount of momentum q_{min} that the projectile needs to transfer to achieve an ionization event ($q_{\text{min}} = \Delta E/v_P$) and the linear momentum conservation equation ($p_R + \mathbf{p}_e = \mathbf{q}$). Since $\boldsymbol{q} = \boldsymbol{K_i} - \boldsymbol{K_f}$ is the momentum transferred by the projectile in the collision process, that is the difference between its initial and final momentum. An ionization event with an electron energy just above threshold can be reached only if the recoil absorbs the linear momentum transfer E_{bind}/v_P along the incidence direction. On the other hand, an ionization event dominated by the projectile-electron interaction, in which the recoil ion plays no role ($p_{\text{rec}} = 0$), can only be produced if the electron is emitted with $p_{\text{elec}} = q$. Since q takes the minimum value E_{bind}/v_P, we find that this value represents a lower limit for the electron momentum. These two limits are linked via the linear momentum conservation equation which eliminates ionization events from region A. To reinforce these statements, we plot in dotted line the linear momentum conservation equation for the particular case in which the electron emission takes place in the z direction [$p_{\text{rec-}z} = (E_{\text{ind}} + p^2_{\text{elec}-z}/2)/v_P\,p_{\text{elec}-z}$]. Electron emission at a given p_{elec} value but at angles other than 0° lead to larger p_{rec} values. Hence, the dotted line provides a phase diagram which highlights the impossibility of having energetic electron emission together with very small recoil momentum.

Moving to region B, we observe that as the impact energy increases, the chance of finding electrons emitted with high energies increases. This has to do with two joint effects: on the one hand, the impact parameter range contraction for increasing impact energies, which favors head-on collisions, and the decreasing role of the electron capture process which at low impact energies removes considerable flux from the ionization channel. This is particularly noticeable at the impact energy of 25 keV, where a sharp barrier in the p_{elec}-p_{rec} space indicates the absence of energetic electron emission and in fact, for the three cases explored, most of the electrons are emitted with $p_{\text{elec}} \leqslant v_P$. In any case, it looks like a simple binary collision between the projectile and the electron with the recoil ion playing the role of a spectator is not a physically sound scenario despite the possibility of $p_{\text{rec}} = 0, p_{\text{elec}} = q$. Needless to say, the present analysis also perfectly applies to the He target case described in the preceding subsection.

In Fig. 10 we show the CTMC-IEV longitudinal and transverse momentum distributions and compare them to the Compton profile. Trends are similar to those already described for He, but in agreement with our observations for electron capture, the transverse distributions do not tend to converge to the Compton profile of Ar($3p$) for increasing impact energies. It seems that the ionization channel is also fed from the low-momentum components of the electron momentum distribution. In concurrence with our analysis for electron capture, we relate this behavior to the very asymmetric charges seen by the electron in the reaction region. Concerning the transverse momentum distributions, the recoil-ion momentum distribution in this direction is nearly

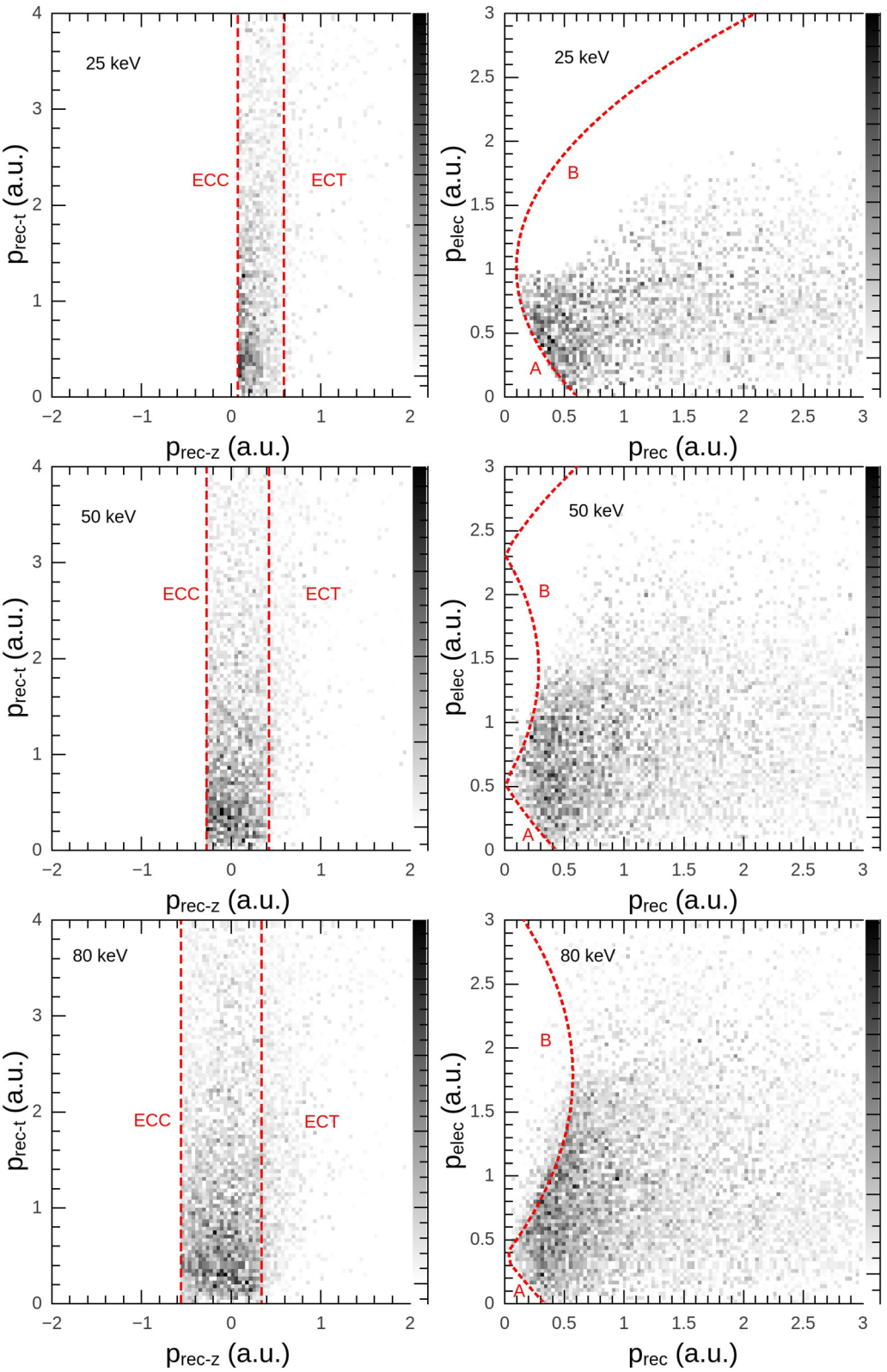

FIG. 9. Theoretical $d^2\sigma/(dp_{elec}dp_{rec})$ and $d^2\sigma/(dp_{rec\text{-}z}dp_{rec\text{-}t})$ of the single-ionization process for 25, 50, and 80 keV H^+ collisions on Ar. The dashed lines indicate the recoil-ion longitudinal momentum values associated with the electron capture to the continuum (ECC) and electron capture to the target (ECT) mechanisms. The dotted line indicates the linear momentum conservation equation for electron emission in the z direction. Predictions within the IEV and IEL models are indistinguishable in this plot.

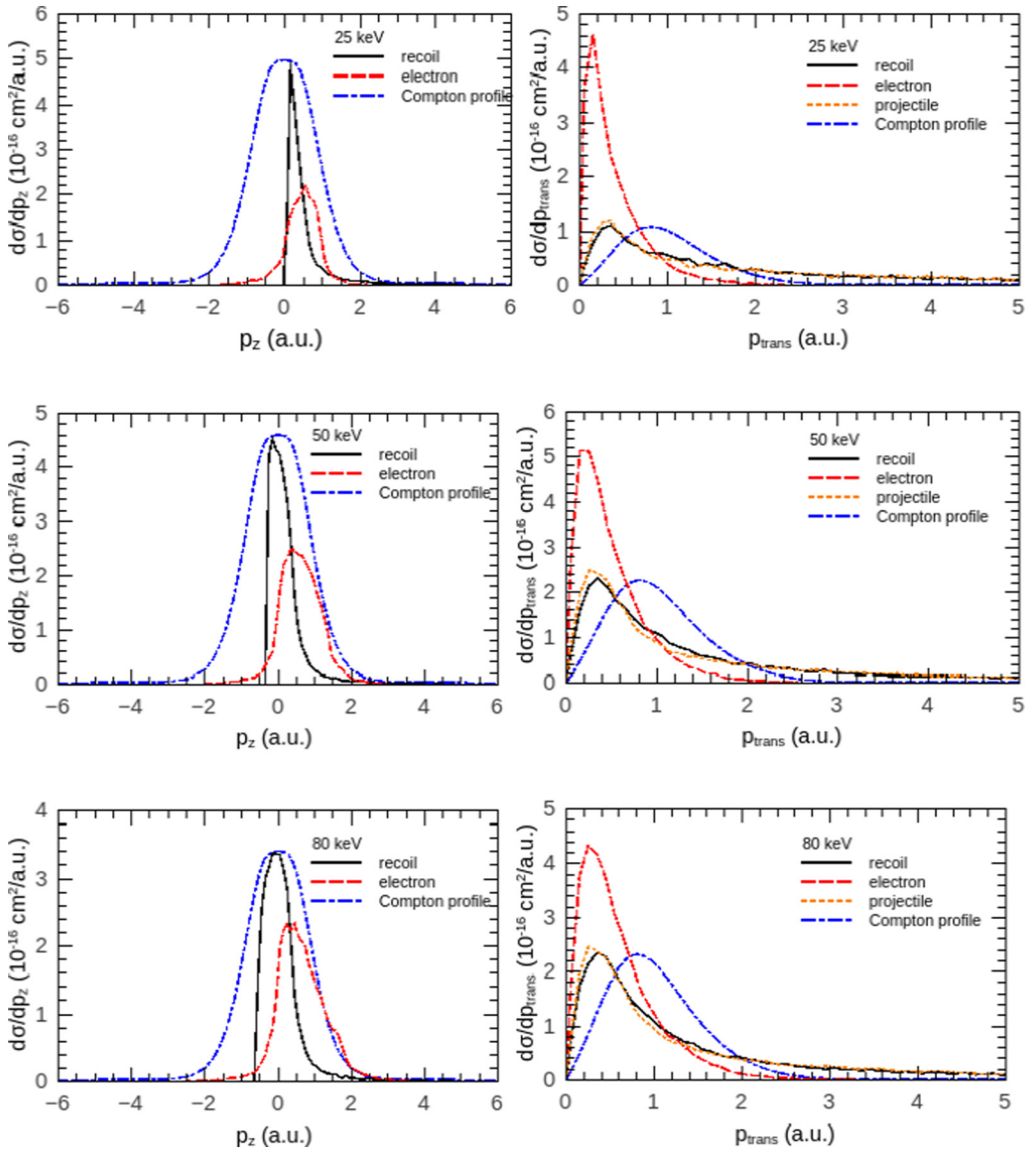

FIG. 10. CTMC-IEV longitudinal and transverse momentum distributions of the single-ionization process for 25, 50, and 80 keV H^+ collisions on Ar.

identical to that obtained for the projectile indicating that the projectile angular dispersion is mainly a consequence of the internuclear interaction, in agreement with our previous findings for He.

V. CONCLUSIONS

In this work the single-electron capture and single-ionization processes have been studied in proton collisions with He and Ar atoms at impact energies in the range 25–100 keV. The main objective of our study was to gain insight on the recoil-ion dynamics for these processes.

To analyze the experimental data, an inversion procedure based on the inverse Abel transform was applied over the transverse component of the recoil target ion measured perpendicular to the Ar gas jet. This procedure allowed us to inspect the electron capture cross sections as a function of the transverse momentum distributions and circumvent the impossibility of incorporating a precooling stage in our COLTRIMS setup for Ar due to its liquefaction at the reservoir.

For proton collisions with He, we found that our recoil-ion transverse momentum distributions for electron capture converged to the Hartree-Fock Compton profile for the initial $1s$ bound state as the impact energy was increased. This trend has been confirmed by our CTMC simulations and shown to be also valid for the single-ionization process. In contrast, our electron capture and ionization recoil-ion transverse momentum distributions for proton collisions with Ar do not converge towards the Compton profile for Ar($3p$). These processes are focused on the portion of the Compton profile corresponding to lower transverse momentum values. We infer from this behavior a clear indication of the present asymmetric interaction of the electron with the target ion and the projectile at small impact parameters.

The analysis of the DDCS in terms of the electron and recoil momentum $[d^2\sigma/(dp_{\rm elec}dp_{\rm rec})]$, a representation to

which not much attention has been paid so far, provided a complementary picture of the ionization collision process. In fact, this representation highlights the accessible p_{elec}-p_{rec} space region for a given collision system and impact energy and, in principle, could be of potential use to identify the influence of undesired external fields.

The present findings provide evidence that the recoil ion plays a fundamental role in the processes hereby studied and highlights the importance of achieving an appropriate description of the three-body nature of the collision process in the reaction region.

ACKNOWLEDGMENTS

Work at Universidad Nacional del Sur is supported by Grants No. PGI 24/F059 and No. PIP 112-201101-00749 of CONICET (Argentina).

[1] R. Moshammer, M. Unverzagt, W. Schmitt, J. Ullrich, and H. Schmidt-Böcking, Nucl. Instrum. Methods Phys. Res., Sect. B **108**, 425 (1996).

[2] V. Mergel, R. Dörner, J. Ullrich, O. Jagutzki, S. Lencinas, S. Nüttgens, L. Spielberger, M. Unverzagt, C. L. Cocke, R. E. Olson, M. Schulz, U. Buck, E. Zanger, W. Theisinger, M. Isser, S. Geis, and H. Schmidt-Böcking, Phys. Rev. Lett. **74**, 2200 (1995).

[3] R. Dörner, H. Bräuning, J. M. Feagin, V. Mergel, O. Jagutzki, L. Spielberger, T. Vogt, H. Khemliche, M. H. Prior, J. Ullrich, C. L. Cocke, and H. Schmidt-Bocking, Phys. Rev. A **57**, 1074 (1998).

[4] M. van der Poel, C. V. Nielsen, M.-A. Gearba, and N. Andersen, Phys. Rev. Lett. **87**, 123201 (2001).

[5] J. W. Turkstra, R. Hoekstra, S. Knoop, D. Meyer, R. Morgenstern, and R. E. Olson, Phys. Rev. Lett. **87**, 123202 (2001).

[6] X. Flechard, H. Nguyen, E. Wells, I. Ben-Itzhak, and B. D. DePaola, Phys. Rev. Lett. **87**, 123203 (2001).

[7] S. Otranto, I. Blank, R. E. Olson, and R. E. Hoekstra, J. Phys. B: At., Mol. Opt. Phys. **45**, 175201 (2012).

[8] R. E. Olson and A. Salop, Phys. Rev. A **16**, 531 (1977).

[9] https://www.iter.org.

[10] M. Alessi, D. Fregenal, and P. Focke, Nucl. Instrum. Methods Phys. Res., Sect. B **269**, 484 (2011).

[11] D. Miller, *Free Jet Sources. Atomic and Molecular Beam Methods* (Oxford University Press, New York, 1988), Vol. 14, pp. 14-53.

[12] M. Alessi, N. D. Cariatore, P. Focke, and S. Otranto, Phys. Rev. A **85**, 042704 (2012).

[13] R. Bracewell, in *The Fourier Transform and Its Applications*, 3rd ed., edited by Kevin T. Kane (McGraw-Hill, New York, 2000), p. 351.

[14] M. J. J. Vrakking, Rev. Sci. Instrum. **72**, 4084 (2001).

[15] I. Blank, S. Otranto, C. Meinema, R. E. Olson, and R. Hoekstra, Phys. Rev. A **87**, 032712 (2013).

[16] A. E. S. Green, D. L. Sellin, and A. S. Zachor, Phys. Rev. **184**, 1 (1969).

[17] R. H. Garvey, C. H. Jackman, and A. E. S. Green, Phys. Rev. A **12**, 1144 (1975).

[18] P. J. Martin, K. Arnett, D. M Blankenship, T. J. Kvale, J. L. Peacher, E. Redd, V. C. Sutcliffe, J. T. Park, C. D. Lin, and J. H. McGuire, Phys. Rev. A **23**, 2858 (1981).

[19] M. Schulz, L. An, and R. E. Olson, J. Phys. B: At., Mol. Opt. Phys. **33**, L629 (2000).

[20] M. S. Schöffler, J. Titze, L. Ph. H. Schimdt, T. Jahnke, N. Neumann, O. Jagutzki, H. Schmidt-Böcking, R. Dörner, and I. Mančev, Phys. Rev. A **79**, 064701 (2009).

[21] F. Biggs, L. B. Mendelsohn, and J. B. Mann, At. Data. Nucl. Data Tables **16**, 201 (1975).

[22] B. Hicks, Phys. Rev. **52**, 436 (1937).

[23] J. W. M. DuMond and H. A. Kirkpatrick, Phys. Rev. **52**, 419 (1937).

[24] Th. Weber, Kh. Khayyat, R. Dörner, V. D. Rodríguez, V. Mergel, O. Jagutzki, L. Schmidt, K. A. Müller, F. Afaneh, A. Gonzalez, and H. Schmidt-Böcking, Phys. Rev. Lett. **86**, 224 (2001).

[25] V. D. Rodríguez, Y. D. Wang, and C. D. Lin, Phys. Rev. A **52**, R9(R) (1995).

[26] R. Dorner, V. Mergel, Liu Zhaoyuan, J. Ullrich, L. Spielberger, R. E. Olson, and H. Schmidt-Bocking, J. Phys. B: At., Mol. Opt. Phys. **28**, 435 (1995).

[27] R. E. Olson and J. Fiol, J. Phys. B: At., Mol. Opt. Phys. **36**, L365 (2003).

[28] C. F. Barnett *et al.*, *Atomic Data for Controlled Fusion Research* (Oak Ridge National Laboratory, Oak Ridge, TN, 1977), pp. A.4.14.